F = molal flow rate of either or both phases, moles/min.
K = equilibrium constant
k, k_1, k_2 = reaction-rate constants
M = number of components taking part in the reaction
M' = number of components playing a role in the kinetics
m = number of independent variables
N = total number of stages in a chain
n = number of moles
N_{T1} = total number of moles in the extractive phase
n_{T2} = total number of moles in the reactive phase
p = order of differential or difference equation
R = ratio of the total number of moles in the extractive phase to the total number of moles in the reactive phase, n_{T1}/n_{T2}
S, S' = number of independent stoichiometric relations between the M or M' components
t = time
t_{ER} = time in an extractive reaction batch process
V = volume of the reactor
x_A = mole fraction of component A
x_{A1} = mole fraction of A in the extractive phase
$x_{A_{i1}}$ = mole fraction of A in the extractive phase of the ith reactor stage
α_A = partition coefficient of the component A, x_{A_1}/x_{A_2}
ϵ = factor relating the phase ratio in a reactor to the effluent flow rates, $F_1/F_2 = \epsilon R$

Subscripts

$A, B, C \ldots$ = components $A, B, C \ldots$
i = any stage in a reactor chain
o = initial conditions
T = total moles in either or both phases
1, 2 = extractive and reactive phase respectively

Superscripts

* = chemical equilibrium conditions

LITERATURE CITED

1. Mattern, R. V., Olegh Bilous, and E. L. Piret, *A.I.Ch.E. Journal*, 3, 497 (1957).
2. Trambouze, P. J., and E. L. Piret, *ibid.*, 5, 384 (1959).

Manuscript received January 6, 1959; revision received January 4, 1960; paper accepted January 4, 1960.

Longitudinal Mixing in Fluidization

E. J. CAIRNS and J. M. PRAUSNITZ

University of California, Berkeley, California

Longitudinal mixing properties in liquid-solid fluidized beds were investigated by means of a salt-solution tracer technique. The electrical conductance breakthrough curves were measured with very small electrical conductivity probes for a step-function input of salt-solution tracer. Longitudinal eddy diffusivities were determined for 1.3- and 3.0-mm. lead spheres and 3.2-mm. glass spheres in 2- and 4-in.-diameter beds at a distance of 5 bed diam. from the injector and for various radial positions.

The longitudinal mixing properties are strongly affected by particle concentration; maximum mixing occurs at a fraction voids of 0.7. Longitudinal eddy diffusivity increases with particle density and with decreasing d_p/D ratio. Velocity profiles markedly influence the eddy-diffusivity profiles.

Fluidized systems have been of great interest in industry for the past decade or more and have come into prominence for use as chemical reactors. In most cases the yields of such reactors are highest when the radial mass transfer processes are maximized and the axial mass transfer processes minimized. The complicated hydrodynamic situation in fluidization defies theoretical analysis, except for very simplified and inexact approaches. Consequently there has been increased effort in the direction of definitive experimentation. A few radial-mixing studies have been conducted (*2, 10*), but data on longitudinal mixing in fluidized systems are rare. Gilliland, Mason, and Oliver (*9*) have presented a few data points for longitudinal diffusion in gas-solid fluidization, and these results yield longitudinal Peclet numbers (Ud_p/E) in the range of 0.0005 to 0.0015. Danckwerts *et al.* (*5*) investigated residence times in an industrial fluidized reactor, and their over-all Peclet number was of the order of 0.001.

The purpose of the present work was to determine and to investigate the important variables affecting the longitudinal mixing in liquid-solid fluidized systems. The mathematics of the model used here was originally presented by H. A. Einstein (*8*) in connection with the motion of pebbles in a water stream.

THEORY

The model applied to a packed bed assumes that the particles of packing material are stationary in space and that the fluid at the surface of the packing particles is stationary with respect to the main stream of fluid. If the assumption is made that the main fluid stream is moving rapidly with respect to the particles, then the model would be expected to be applicable to a fluidized bed. However if this assumption is only approximately valid, the mathematical results are still accurately applicable, owing to the central-limit theorem, provided that a large enough number of events is considered, that is, that the bed is of sufficient length.

The statistical model, which is discussed in detail elsewhere (*1, 11*), considers the motion of tracer corpuscles in the mainstream fluid. The corpuscles move according to a repeating pattern of a *motion phase* followed by a *rest phase*. A very small amount of time is required for the motion phase but the rest phase requires much longer. Thus the tracer corpuscles move, then rest, then move, etc. The rest phase may be thought of as taking place at the various stagnation points at each packing particle and in the eddies and the relatively stagnant points immediately downstream of the particles. The motion phase occurs during the rapid flow between particles.

E. J. Cairns is with General Electric Company, Schenectady, New York.

The probability density function for the position of the tracer corpuscle with respect to longitudinal distance and time after one double phase is

$$p(z,t')dzdt' = e^{-t'-z}dzdt' \quad (1)$$

By applying this probability density function to a consecutive set of motion and rest phases which result in the tracer corpuscle being found at the position $z = N$ at $t' = T$, and considering all possible paths for arriving at N at T, one arrives at the expression

$$F_{N(T)} = \int_0^T e^{-N-T}\, \mathrm{I}_0(2\sqrt{NT})\, dT \quad (2)$$

The definition of $F_{N(T)}$ in Equation (2) corresponds to a step function tracer input.

The important assumptions involved in the above derivation are that the velocity profile over the region of interest is flat, the probability of a corpuscle coming to rest is independent of longitudinal position, and the time lapse during the motion phase is short.

Equation (2) may well be approximated (*12*) by

$$F_{N(T)} = \frac{1}{2}\left[1 + \mathrm{erf}\left(\sqrt{T} - \sqrt{N} - \frac{1}{8\sqrt{T}} - \frac{1}{8\sqrt{N}}\right)\right] \quad (3)$$

The parameters T and N are related to the more familiar parameters of eddy diffusivity and time by

$$N = \frac{ZU}{E} \quad (4)$$

$$T = \frac{U^2 t}{E} \quad (5)$$

$$T/N = \left(\frac{Ut}{Z}\right) \equiv \theta \quad (6)$$

Equation (4) is in essence a definition of the eddy diffusivity in terms of the Einstein statistical equations. If $F_{N(T)}$ is plotted against (T/N) for an assumed N, the familiar breakthrough type of curve is obtained.

A very convenient method of evaluating N (and hence the Peclet group which is equal to $N\, d_p/Z$) is to obtain the slope of the breakthrough curve at the point $T/N = 1$, since from Equation (2)

$$\left(\frac{\partial F}{\partial (T/N)}\right)_{T/N=1} = N\frac{I_0(2N)}{e^{2N}} \quad (7)$$

For large N one obtains

$$\left(\frac{\partial F}{\partial (T/N)}\right)_{T/N=1} = \frac{\sqrt{N}}{2\sqrt{\pi}} \quad (8)$$

$$N = 4\pi\left(\frac{\partial F}{\partial (T/N)}\right)^2_{T/N=1} \quad (9)$$

Equation (7) gives a very rapid method of determining Peclet groups from experimental data. Other methods (*4, 6, 7, 14, 15, 17, 20*) require considerably more extensive calculations.

EXPERIMENTAL

The discussion above indicates that it is desirable to use a tracer technique for studying longitudinal mixing behavior in fluidized beds. Since the fluid velocity is relatively high, ordinary sampling procedures are unsatisfactory; a continuous monitoring procedure would be very desirable, since transients in the system are to be followed. The electrical conductivity of an electrolytic solution is very nearly proportional to the concentration of the electrolyte, and the time lag of electrical conductivity measurements is negligible. Therefore the electrical conductivity method was chosen for continuously following the liquid-phase mixing behavior by injecting a sodium nitrate solution into an aqueous main stream.

General Flow Apparatus

A schematic flow diagram of the equipment is shown in Figure 1. Water is obtained from a constant-head tank, metered, and pumped by means of a regenerative type of turbine pump into the flow distributor, which causes the water to have a flat velocity profile. From the distributor the water passes up into the flow-development section, which is an 8-in. length of tube having the same diameter as the test section and packed with 2-mm. glass spheres. The injector head is mounted directly above the flow-development section, and the test section is immediately above the injector head.

The upper surface of the injector head supports a screen which in turn supports the fluidized bed. The space below the screen and above the flow-development section is also packed with spheres. Above the test section is a particle disengaging section, which is an open tube, 8 in. long, which overflows into a tank and drainage system.

The apparatus was designed in such a manner that various diameters and heights of test sections could be be employed. Two-and 4-in.–diameter test sections 2 ft. long were studied in this work. The diameters and specific gravities of the particles studied were 3.2 mm., $\rho = 2.45$; 3.0 mm., $\rho = 11.3$; 1.3 mm., $\rho = 11.3$.

Electrical Conductivity Probes

The probe tip which holds the electrodes was constructed from a Bakelite type of material in cylindrical form, 3 mm. in diameter. The rod contains a slot 7 mm. deep and 1 mm. wide. On each side of the slot a circular platinum electrode 1 mm. in diameter is mounted less than 1 mm. from the probe tip. Wires from the electrodes are passed through the tip and into the probe body of ⅛-in. diameter stainless steel tube. The leads are passed through the tube and connected to the electronic apparatus. These probes are able to measure the conductance of a very small volume of fluid (about 1 cu. mm.) and to trace that conductance with a negligible time lag. The stagnation point at the slot end is relatively far from the electrodes in order that there may be negligible stagnation or holdup effects on the conductance reading.

The mounting device for the probes was constructed such that the probes can monitor the conductance at any Z level in the bed and at any angular orientation around the axis. The radial positions can be obtained in multiples of $r_0/12$. The mounting device dips into the bed from above and fits snugly against the tube walls, causing a minimum of disturbance to the flow. The probe tips are at all times at least 4⅞ in. from the nearest portion of the probe support.

Electronics

The determination of the electrical conductance of the solution between the electrodes of the probe described above must be a continuous one, and hence standard bridge networks could not be used. Figure 2 schematically shows the basic network. The oscillator was voltage stabilized and supplied a 20-kc. voltage. A current-sensing resistor r was selected so that it would always be less than 0.01 R where R is the resistance of the solution in the conductivity probe. Therefore V_r is very nearly directly proportional to $(1/R)$, which is the conductance of the solution.

The signal V_r was then fed to an amplifier and demodulator network. The output of the amplifier demodulator was a varying d.c. voltage directly proportional to the conductivity of the solution in the probe.

The amplified signal was used to drive a mirror type of galvanometer in the Heiland type 906 Visicorder. The Visicorder had a flat frequency response up to about 300 cycles/sec. and hence could be used to study the transients of interest in this work.

The amplifier-demodulator network was able to accommodate six simultaneous signals from the probes and also delivered to the recorder these signals as well as a 60-cycle timing pip and a start pip, which was electronically placed on the chart when the step function of tracer solution was turned on or off. The start and timing pips are discussed in more detail elsewhere (*1*). The timing pip allows accurate calculation of the chart speed; the start pip allows calculation of time lapsed since the step-function injection.

Injection System

The tracer injection system consisted of a piston and cylinder driven by a geared-down variable-speed drive unit. The variable-speed drive was calibrated so that an accurately known volume of liquid was being delivered per unit of time for a given drive setting. The fluid from the cylinder could be delivered to either of two places, depending on the position of the solenoid-valve switch. The fluid could be fed back to the reservoir from which it originally came or to the injector head at the base of the test section.

The injector head for the 4-in.–diameter test section had one-hundred fifty-six hypodermic needles (18 gauge) placed on a square lattice having 9/32-in. spacing.

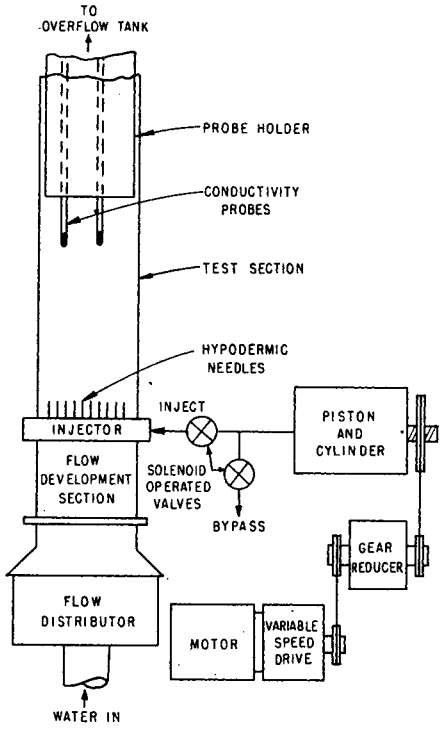

Fig. 1. Schematic flow diagram.

The head for the 2-in. test section had thirty-seven needles on the same arrangement. Calculations, which are described in detail elsewhere (*1*), showed that these injectors provide very nearly a plane source of tracer. At an axial distance of less than 5 particle diam. from the needle tips, the ripple in the concentration contour map for that Z level was only 9% of the average concentration.

The solenoid-valve arrangement mentioned above allowed a very sharp wave front of injectant to be sent into the test section or, conversely, the very rapid diversion of the injectant stream from the test section. This step-function property of the injection system allowed the use of the equations in the theory section for data analysis.

Procedure

During the time allowed for the fluidized bed to come to equilibrium the injector drive speed was determined in such a way that the linear injectant velocity at the needle tips was equal to the average main stream linear velocity (U_o/ϵ).

The injectant was fed into the test section until steady state was reached, as indicated by constant conductivity readings for all probes on the Visicorder. The amplifier gains were adjusted so that the traces on the chart were in certain relative positions that permitted each trace to be identified with the corresponding probe and probe position in the bed. The injectant stream was suddenly diverted from the column by activating the solenoid valve. At this same instant the start pip was electronically placed on the chart. The breakthrough curves for all the probes were traced to their final values, characteristic of tap water. The temperature of the water was recorded along with flow rate, injection rate, bed height and diameter,

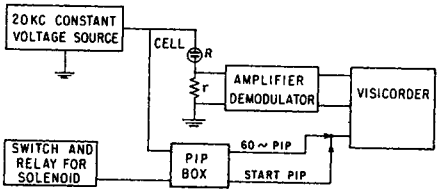

Fig. 2. Block diagram for one channel.

and weight, density, and diameter of the packing material.

Similar data were collected for various flow rates (or fraction voids) for each of the particle sizes in both 4- and 2-in. test sections.

REDUCTION OF DATA

For convenience and speed in the reduction of data it is advantageous to use an expression of the form of Equation (9). However from the raw data it is not possible to obtain the location of the point $T/N = 1$ without trial and error. For this reason it is convenient to take the slope of the breakthrough curve on the chart at some other point which can be located without trial and error; such a point is $F = 1/2$.

Knowing the slope at the point $F = 1/2$ one can calculate the slope at the point $T/N = 1$ by use of the derivative of Equation (2) with respect to (T/N). For an assumed N the corresponding T for $F = 1/2$ may be calculated from Equation (3), and then these values of T and N are inserted into the derivative of Equation (2) with respect to (T/N). The value of the slope for $(T/N) = 1$ is obtained from Equation (7) for this same assumed N. The ratio of the two slopes is defined as

$$\beta = \frac{\left(\frac{\partial F}{\partial \theta}\right)_{\theta=1}}{\left(\frac{\partial F}{\partial \theta}\right)_{F=1/2}} \qquad (10)$$

Therefore $(\partial F/\partial\theta)_{\theta=1}$ may be obtained from $(\partial F/\partial\theta)_{F=1/2}$.

Since Equation (9) is only approximate, it is desirable to have the relationship between the exact Equation (7) and the approximate Equation (9). This relationship is given in the form

$$N = 4\pi \left(\frac{\partial F}{\partial \theta}\right)^2_{\theta=1} \cdot \frac{1}{\alpha^2}$$

$$= 4\pi \left(\frac{\partial F}{\partial \theta}\right)^2_{\theta=1} \left[\frac{\exp(2N)}{I_o(2N) \cdot 2\sqrt{\pi N}}\right]^2 \qquad (11)$$

which also defines α for the case $T = N$.

Since the electrical conductivity of the sodium nitrate solution is not exactly proportional to the concentration of the sodium nitrate, an additional correction factor is needed. The form of the empirical equation relating C to L is

$$C = aL^b \qquad (12)$$

The correction factor takes the form

$$\left[b\left(\frac{L}{L_\infty}\right)^{b-1}\right]_{F=1/2} = \left[b\left(\frac{1}{2}\right)^{\frac{b-1}{b}}\right] \qquad (13)$$

which is a weak function of temperature. The final equation used in reducing the data is

$$N_{Pe'} = 4\pi\left\{\frac{dy}{dx}\ \frac{b}{1.02}\left(\frac{L}{L_\infty}\right)^{b-1}\left(\frac{Z}{U_i}\right)\left(\frac{dx}{dt}\right)\right\}^2_{F=1/2}\left(\frac{d_p}{Z}\right)\Delta^2 \qquad (14)$$

The term in the large brackets is $(dF/d\theta)_{F=1/2}$, where $\theta = T/N$ or $[(U_i t)/Z]$. The value of 1.02 is a correction factor for a slight nonlinearity in the Visicorder which must be incorporated in the determination of the slope of the breakthrough curve. This nonlinearity however is negligible in determining the point $F = 1/2$.

Equation (14) gives a rapid means for reducing data from the experimental step-function method. Details of its use and derivation have been previously presented, along with a plot of (Δ^2-1) vs. $(\partial F/\partial\theta)^2_{F=1/2}$ (*1*). The line velocity is found from the breakthrough curve. Since for $F = 1/2$, $\theta = U_i t/Z \approx 1$, $U_i = Z/t$ where t corresponds to the point $F = 1/2$. The error in this assumption is usually less than 1%.

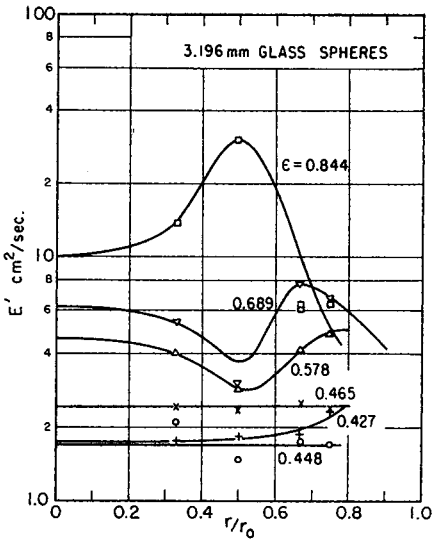

Fig. 3. Longitudinal eddy-diffusivity profile, 2-in. tube.

RESULTS

As discussed previously (*1, 2*), velocity profiles in packed and fluidized beds tend not to be flat. In a liquid-

solid fluidized bed the velocity distribution deviates from flatness much more than does the distribution for packed beds; these nonflat velocity profiles give rise to the corresponding nonflat eddy-diffusivity profiles shown in Figures 4 and 5.

The experiments described here indicate that under the conditions of greatest deviation from a flat velocity profile (±20%) the ratio of eddy diffusivities (E_z/E_r) is about 20 to 30. The longitudinal concentration gradients are one or two orders of magnitude steeper than any radial gradients that could develop, and hence the rate of longitudinal mass transfer is much greater than the rate of radial mass transfer; the ratio of axial to radial tracer flux is estimated as being at least 10^2. Thus the radial mass transfer is expected to have a negligible effect on the axial diffusivities reported here.

Figure 3 presents a sample set of eddy-diffusivity profiles showing the data points. The scatter is representative of the glass particle systems; the data for the lead particle systems scattered a little more. Figures 4 and 5 present the results for the various studies in terms of the eddy diffusivity as calculated from the Peclet group $E' = (U_t d_p)/N_{Pe}'$. The numbers in parentheses near each curve give the fraction voids as calculated from the bed height, weight and density of particles, and bed diameter. Tabulations of the data from which the curves were drawn are available elsewhere (*1*).

The left-hand portion of Figure 4 indicates that the 1.3-mm.–diameter lead spheres in the 4-in. tube yield eddy-diffusivity profiles very similar in shape to the velocity profiles reported previously (*2*). The impression given by these profiles is that the eddy diffusivity is not a function of radial position. The two profiles which deviate most from being flat are at fraction voids very near to one another (0.510 and 0.547). There is no special reason to believe that there is a sudden and extensive change in the eddy-diffusivity profile in this short range of fraction voids. Taken together these two curves would predict a resultant flat profile, consistent with the rest of the set. The very small d_p/D ratio (0.013) combined with the high particle-to-fluid density ratio (11.3) yields flat velocity profiles as well as flat eddy-diffusivity profiles. The eddy diffusivity reaches a maximum in the vicinity of $\epsilon = 0.66$.

The central portion of Figure 4 shows that there is an influence due to the wall and the nonflat velocity profile. When one starts with $\epsilon = 0.400$ (packed bed), the eddy diffusivity increases as the wall is approached. The

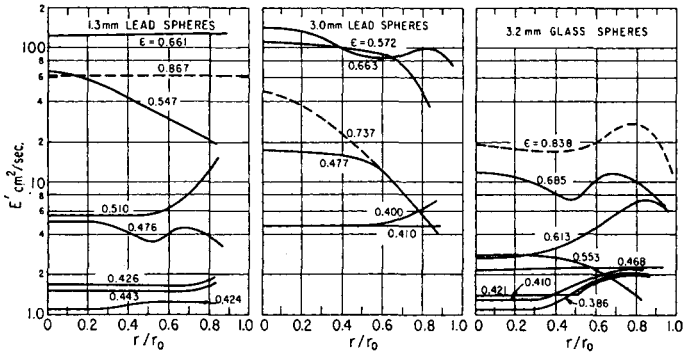

Fig. 4. Longitudinal eddy-diffusivity profiles in fluidization, 4-in. tube.

same is true for the velocity. This increase is undoubtedly due to a rise in the fraction voids as the wall is approached. As the bed is expanded to incipient fluidization ($\epsilon = 0.410$), the eddy-diffusivity profile becomes flat (corresponding to a flat velocity profile), and as the bed finally fluidizes ($\epsilon = 0.477$), there develops a well-defined nonflat eddy-diffusivity profile with a maximum at the center. An increase in the bed expansion changes the particle circulation pattern, velocity profile, scale and intensity of turbulence, and local fraction voids in such a manner that humps develop in the eddy-diffusivity profiles at $\epsilon = 0.572$ and $\epsilon = 0.663$.

The profiles in the right-hand portion of Figure 4 for glass particles of 3.2 mm. show the same general behavior at low fraction voids as those for the central portion for lead particles. However since lower velocities are required for the fluidization of the glass, and lower scales of turbulence are expected, lower eddy-diffusivity values would be expected than for the corresponding fraction voids in the case of lead. The humps caused by the particle circulation patterns are more predominant in the case of the glass particles; this is not surprising since the particle circulation is qualitatively different in the case of glass from that in the case of lead (*1*).

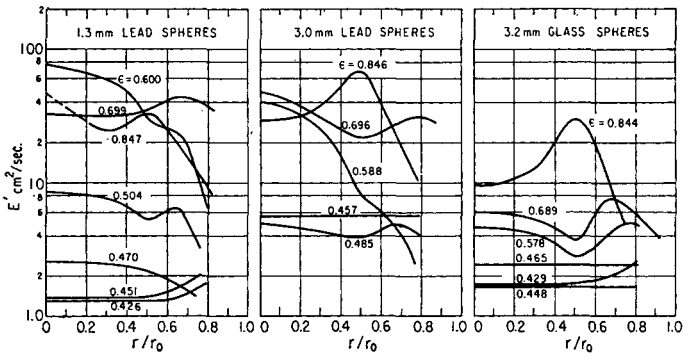

Fig. 5. Longitudinal eddy-diffusivity profiles in fluidization, 2-in. tube.

The left-hand portion of Figure 5 presents the results for the 1.3-mm. lead particles in the 2-in. test section at the corresponding distance from the injector in terms of Z/D. There are large deviations from flatness in the

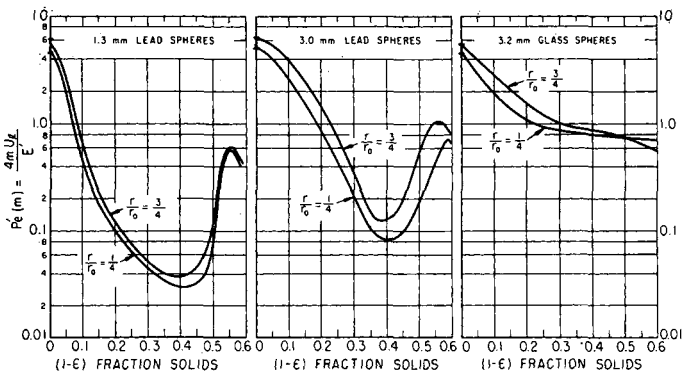

Fig. 6. Longitudinal Peclet numbers in fluidization, 4-in. bed.

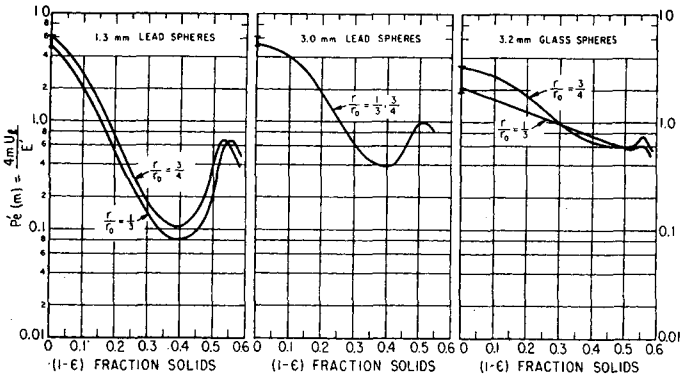

Fig. 7. Longitudinal Peclet numbers in fluidization, 2-in. bed.

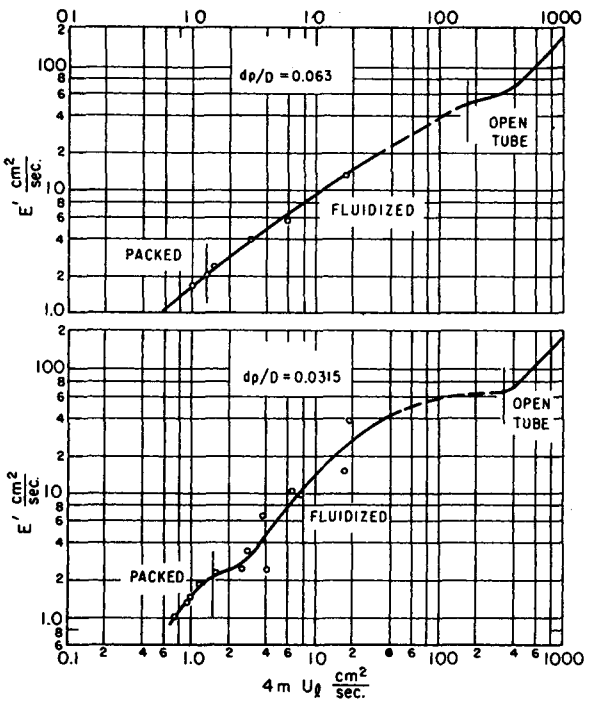

Fig. 9. Longitudinal eddy diffusivities in fluidization, glass spheres, d_p = 3.196 mm.

eddy-diffusivity profiles. Much better agreement between sets of profiles is obtained if they are compared on a basis of comparable d_p/D ratios rather than on the basis of particle diameter alone. When one uses this reasoning, the left-hand portion of Figure 5 agrees very well with the central portion of Figure 4. Again a maximum in eddy diffusivity occurs corresponding to fraction voids of 0.6 or 0.7.

The central portion of Figure 5, presenting results for 2.96-mm. lead spheres in the 2-in. test section, shows behavior similar to the other systems having comparable d_p/D ratios for the same bead density.

Finally the right-hand portion of Figure 5 shows the results for the 3.2-mm. glass beads in the 2-in. test section. These results show similarities to those for the same type of packing in the larger tube in that the humps occur at the same distance from the wall in terms of the number of bead diameters from the wall. Generally the eddy diffusivity is lower in the smaller tube owing to the more restricted circulation of the beads in the smaller tube.

To show the effects of fraction solids $(1-\epsilon)$ on the Peclet group $[N_{Pe'(m)} = (4mU_t)/E]$, Figures 6 and 7 were prepared. The symbol m refers to the hydraulic radius as extended by Wilhelm (*17, 21*) and is defined as m = volume of fluid/wetted area. If the characteristic length term is defined in this manner, the Peclet group may vary continuously from the packed-bed value, where m is determined primarily by the packing size to the open-tube value, where $4m$ is equal to the tube diameter.

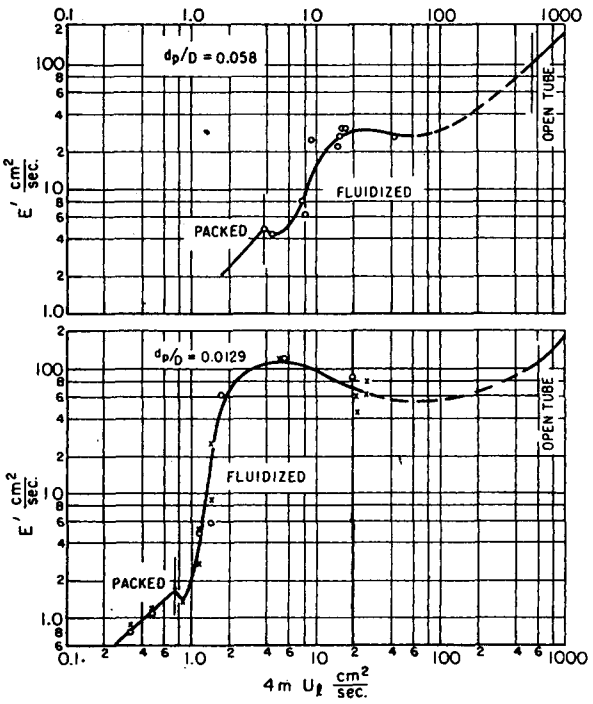

Fig. 8. Longitudinal eddy diffusivities in fluidization, lead spheres, d_p = 2.96 mm.

When one considers Figure 6, it is apparent that there is slightly better mixing (lower Peclet group) toward the center of the tube for given average fraction voids. When compared with the fraction-voids effect, however, the effect of radial position is rather small in most cases, especially where ρ_p/ρ_f is large. The minimum in $N_{Pe'(m)}$, when present, occurs at $\epsilon = 0.6$. The effect of using $4m$ as a length term in $N_{Pe'(m)}$ tends to shift this minimum to the right, and if $N_{Pe'} = (U_t d_p)/E'$ were plotted against fraction solids, the minimum would occur at $\epsilon = 0.7$, where the corresponding minimum in radial Peclet group is situated (*1*).

Figure 7 contains plots similar to those of Figure 6; however these are for the 2-in. test section. There is a very good correspondence between the central portion of Figure 6 and the left-hand portion of Figure 7, again bringing out the importance of the d_p/D ratio in determining the mixing behavior in a fluidized bed.

All open-tube values $(1-\epsilon = 0)$ were obtained from Tichacek *et al.* (*19*) at velocities corresponding to the terminal velocity of the particle in question. The hydraulic radius is used

as the characteristic length because it is easily calculated from readily available data and provides a continuous function in going from the packed bed to the empty tube.

For comparing and summarizing the mixing behavior of various systems one may turn to the theories of turbulent mixing to suggest the characteristic parameters for correlating eddy-diffusion coefficients. The Einstein statistical model shows that the longitudinal eddy diffusivity is the product of a characteristic length term and a characteristic velocity term. Prausnitz (*18*), on the basis of a mixing-length model, comes to the same conclusion. The eddy diffusivity should therefore be expressed as a function of the product of a characteristic length term and a characteristic velocity term. The characteristic length term proposed here for simplicity is the hydraulic radius; the velocity term proposed is the line velocity discussed previously (*1, 2, 3*).

Figures 8 and 9 show representative results for some of the systems studied, plotted in the manner suggested by the above discussion. The remainder of the results are available elsewhere (*1*). The results for some of the lead particle systems as shown in Figure 8 indicate that there is a very rapid increase in the eddy diffusivity with increase in mU_l just after fluidization has set in. At mU_l values higher than those corresponding to fraction voids of about 0.7, there is a relatively small change in the eddy diffusivity for a given change in mU_l, until the open-tube value is approached. For the $d_p/D = 0.058$ curve there is a wall effect in restricting the particle motion causing the eddy diffusivity to be lower than that for the d_p/D ratio of 0.013 at the corresponding fraction voids (or corresponding mU_l).

Figure 9 shows similar results for the glass packing. There is a noticeable difference between Figures 8 and 9 in that the denser particles show a much more pronounced effect in increasing eddy diffusivity. For a d_p/D ratio of 0.063 and ρ_p of 2.45 g./cc. the line joining the packed- and open-tube values shows very little curvature. For d_p/D of 0.0315 the effect is increased somewhat but is not equivalent to that for lead packing for the same d_p/D ratio.

SUMMARY AND CONCLUSIONS

The longitudinal mixing properties in liquid-solid fluidized beds were investigated by means of a step function response technique. The longitudinal eddy diffusivities were determined for glass and lead particles in water at various d_p/D ratios, fraction voids, and radial positions at an axial level of about 5 bed diam.

The experimental results show that the eddy diffusivity is strongly affected by the density and concentration of the particles in the fluidized beds. The mixing results are consistent with the fact that the fluidized bed may be considered as a transition between a packed bed and an open tube.

NOTATION

a = constant in Equation (12)
b = constant in Equation (12)
C = salt concentration
d_p = packing-particle diameter
D = test-section diameter
E = eddy diffusivity (analogous to molecular diffusion constant), based on average velocity
E' = eddy diffusivity based on line velocity
F = dimensionless concentration $= C/C_\infty$
I_o = Bessel function of zero order and first kind of an imaginary argument
L = conductance
m = hydraulic radius = volume of fluid/wetted area
N = dimensionless longitudinal distance $= ZU/E$
p = probability density
N_{Pe} = longitudinal Peclet number $= U_o d_p/\epsilon E$
N_{Pe}' = longitudinal Peclet number based on line velocity $= U_l d_p/E'$
$N_{Pe(m)}$ = longitudinal Peclet number based on average velocity and hydraulic radius $= 4mU_o/E\epsilon$
$N_{Pe'(m)}$ = longitudinal Peclet number based on line velocity and hydraulic radius $= 4mU_l/E'$
r = radial position
r_o = radius of test section
t = time
t' = dimensionless time variable
T = dimensionless time unit $= U^2t/E$
$\frac{T}{N}$ = dimensionless time $= Ut/Z$
U = characteristic fluid velocity (general)
U_l = line velocity of fluid $= 1/Z \int_o^z U_p\, dZ$
U_o = superficial fluid velocity (based on open-tube cross section).
U_p = velocity of the fluid observed at a point
V = voltage of signal to recorder
x = distance on recorder chart parallel to time axis
y = displacement of recorder trace from its no-signal position
z = dimensionless longitudinal position
Z = distance of observation point from injection plane

Greek Letters

α = correction factor $= [2\sqrt{N}\, I_o(2N)]/[\exp(2N)]$ for $T = N$
β = $[(\partial F/\partial\theta)_{\theta=1}]/[(\partial F/\partial\theta)_{F=1/2}]$ = a correction factor
Δ = over-all correction factor $= \beta/\alpha$
ϵ = fraction voids
θ = dimensionless time $= T/N = Ut/Z$
ρ = density, g./cc.

Subscripts

∞ = value prevailing during steady state tracer injection
f = fluid
p = particle

Superscripts

'(prime) = based on line velocity

LITERATURE CITED

1. Cairns, E. J., dissertation, Univ. Calif., Berkeley (1959).
2. ———, and J. M. Prausnitz, *Ind. Eng. Chem.*, **51**, 1441 (1959).
3. ———, *Chem. Eng. Sci.*, to be published.
4. Carberry, J. J., and R. H. Bretton, *A.I.Ch.E. Journal*, **4**, 367 (1958).
5. Danckwerts, P. V., *et al.*, *Chem. Eng. Sci.*, **3**, 26 (1954).
6. Deisler, P. F., and R. H. Wilhelm, *Ind. Eng. Chem.*, **45**, 1219 (1953).
7. Ebach, E. A., and R. R. White, *A.I.Ch.E. Journal*, **4**, 161 (1958).
8. Einstein, H. A., dissertation, Eidgenossische Technische Hochschule, Zürich, Switzerland (1937).
9. Gilliland, E. R., E. A. Mason, and R. C. Oliver, *Ind. Eng. Chem.*, **45**, 1177 (1953).
10. Hanratty, T. J., George Latinen, and R. H. Wilhelm, *A.I.Ch.E. Journal*, **2**, 372 (1956).
11. Jacques, G. L., and Theodore Vermeulen, *A.I.Ch.E. Journal*, to be published.
12. Klinkenberg, Adrian, *Ind. Eng. Chem.*, **46**, 2285 (1954).
13. ———, and F, Sjenitzer, *Chem. Eng. Sci.*, **5**, 258 (1956).
14. Kramers, H., and G. Alberda, *ibid.*, **2**, 173 (1953).
15. Lapidus, Leon, and N. R. Amundson, *J. Phys. Chem.*, **56**, 984 (1952).
16. Levenspiel, Octave, and W. K. Smith, *Chem. Eng. Sci.*, **6**, 227 (1957).
17. McHenry, K. W., and R. H. Wilhelm, *A.I.Ch.E. Journal*, **3**, 83 (1957).
18. Prausnitz, J. M., *ibid.*, **4**, 14M (1958).
19. Tichacek, L. J., C. H. Barkelew, and Thomas Baron, *ibid.*, **3**, 439 (1957).
20. Van der Laan, E. T., *Chem. Eng. Sci.*, **7**, 187 (1958).
21. Wilhelm, R. H., *Chem. Eng. Progr.*, **49**, 150 (1953).

Manuscript received April 24, 1959; revision received September 18, 1959; paper accepted October 2, 1959.